Geophysical Journal International

Geophys. J. Int. (2019) **219,** 2165–2173
Advance Access publication 2019 September 27
GJI Seismology

doi: 10.1093/gji/ggz429

Spatio-temporal seismic velocity variations associated to the 2016–2017 central Italy seismic sequence from noise cross-correlation

Gaia Soldati,[1] Lucia Zaccarelli[2] and Licia Faenza[3]

[1] *Istituto Nazionale di Geofisica e Vulcanologia, sezione di Roma*1*, Roma, Italy. E-mail: gaia.soldati@ingv.it*
[2] *Istituto Nazionale di Geofisica e Vulcanologia, sezione di Bologna, Bologna, Italy*
[3] *Istituto Nazionale di Geofisica e Vulcanologia, sezione ONT, Bologna, Italy*

Accepted 2019 September 25. Received 2019 September 10; in original form 2018 December 27

SUMMARY

We investigate the temporal changes of crustal velocity associated to the seismic sequence of 2016–2017, which struck central Italy with a series of moderate to large earthquakes. We cross-correlate continuous recordings of 2 yr of ambient seismic noise from a network of 28 stations within a radius of 90 km around Amatrice town. We then map the spatio-temporal evolution of the velocity perturbations under the effect of subsequent earthquakes. Coinciding with each of the three main shocks of the sequence we observe a sudden drop of seismic velocity which tends to quickly recover in the short term. After the end of the strongest activity of the sequence, the coseismic velocity changes display gradual healing towards pre-earthquake conditions following a quasi-linear trend, such that by the end of 2017 about 75 per cent of the perturbation is recovered. The spatial distribution of the velocity drop fluctuates with time, and the area that shows the most intense variations beyond the ruptured fault system elongates in the NE direction. This zone roughly corresponds to a region of foredeep sedimentary deposits consisting of highly hydrated and porous sandstones, which respond to the passage of seismic waves with increased pore pressure and crack number, leading to a reduction of the effective relative velocity.

Key words: Time-series analysis; Seismic interferometry; Seismic noise.

1 INTRODUCTION

Starting from August 2016, central Italy has been hit by a sequence of destructive earthquakes, which activated an approximately 80-km-long and 20-km-wide fault system along a portion of the Apenninic belt, filling the gap between the northern 1997 Colfiorito and the southern 2009 L'Aquila events. The whole sequence lasted several months and was confined within the upper 10–12 km of the crust (Marchetti *et al.* 2016; Michele *et al.* 2017), with main shocks showing NW–SE striking normal faulting, consistent with the direction of active extension in this sector of the Apennines (Serpelloni *et al.* 2005; Devoti *et al.* 2017).

No significant foreshock activity on the main fault plane has been identified from the spatio-temporal analysis of the seismicity in the area during the year preceding the beginning of the sequence (Marzorati *et al.* 2016; Michele *et al.* 2016). The first main shock (moment magnitude M_w 6.0) occurred on the 24 August 2016 close to the town of Accumuli, and was followed by tens of thousands of aftershocks, over a 30-km-long area. The largest aftershock (M_w 5.4) happened only 1 hr later about 10 km further north, close to the town of Norcia. For at least 10 d, the sequence was very active with a series of earthquakes with magnitude larger than 4.0, causing devastation in the town of Amatrice (Chiaraluce *et al.* 2017). The two large events (M_w 5.4 and 5.9) on October 26, near Ussita and Visso, activated another 20-km-long segment in the NW direction. Then, the activity reached the climax on October 30, when a M_w 6.5 earthquake, the largest of the sequence, hit right in between Norcia and Ussita. On 18 January 2017, the seismic activity grew again with the occurrence of four moderate-magnitude earthquakes ($5.0 \leq M_w \leq 5.5$) near the town of Campotosto, about 10 km in the SW direction from Amatrice.

Changes in seismic velocity in the Earth's crust have been documented in many instances, both in connection with tectonic and volcanic processes. The ambient noise correlation technique has become the predominant method of measuring these velocity changes in recent years, since ambient noise is continuously recorded and achieved for most networks. The method is very versatile and allows several applications, like the detection of coseismic changes and post-seismic relaxation after major earthquakes (Brenguier *et al.* 2008; Hobiger *et al.* 2012; Soldati *et al.* 2015), of possible precursors of volcanic eruptions (Brenguier *et al.* 2011; Obermann *et al.* 2013; Sanchez-Pastor *et al.* 2018), and of interactions between seismic events and the state of Earth's crust in volcanic areas (Brenguier *et al.* 2014; Taira & Brenguier 2016).

Here, we apply this approach to 2 yr of continuous seismic records from 28 seismic stations (Fig. 1, red and blue triangles) to monitor in

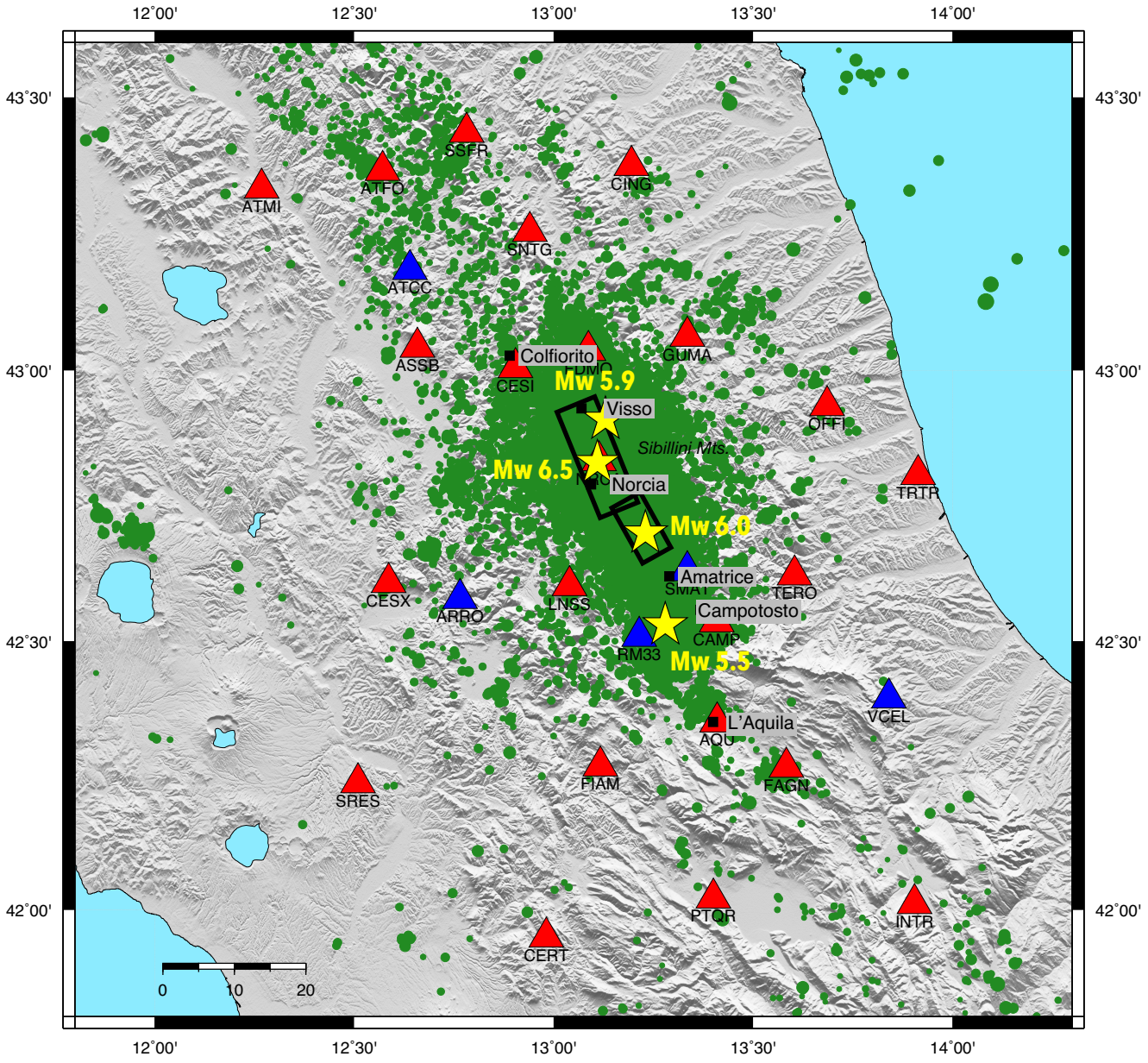

Figure 1. Map of the central Apennines showing the seismic stations considered in this study: red triangles refer to broad-band stations and blue triangles to short period ones. Yellow stars correspond to the location of the four $M_w \geq 5.5$ earthquakes of the sequence and black rectangles the faults plane projection of the two largest events (M_w 6.0 of 24/08/16 and M_w 6.5 of 30/10/16). Green dots represent the seismicity in the 2 yr between January 2016 and December 2017.

terms of relative velocity variations the coseismic and post-seismic responses to the occurrence of the largest earthquakes of the 2016–2017 central Italy sequence. In addition, we map the time evolution of the spatial distribution of the relative velocity variations by interpolating the values of the velocity drop on the single stations computed at different times. A tentative comparison is made with respect to the results obtained from the analysis of the 2009 L'Aquila earthquake sequence by Zaccarelli *et al.* (2011) and Soldati *et al.* (2015).

2 DATA AND METHOD

We select from the catalogue of the Italian National Seismic Network (INSN, http://www.fdsn.org/networks/detail/IV/) and of the Mediterranean Very Broadband Seismographic Network (*MedNet* http://www.fdsn.org/networks/detail/MN/), the stations located within 90 km of Amatrice, approximately in the central part of the area affected by the earthquake sequence. We operate a further selection based on data quality (duration of gaps in the recordings lower than approximately 20 per cent of the total length) and to assure a uniform density of stations in the region considered. Figs S1 and S2 show the map of all the stations present in the area (in red the ones selected for this analysis) and the data availability. We compile a data set composed of continuous seismic recordings from 28 stations, 5 of which are short-period and 23 broad-band (blue and red triangles in Fig. 1), with data from January 2016 to December 2017. Due to the difference in sensors, the pre-processing of the data must include a correction for the instrument response in addition to waveforms syncronization, gap interpolation, spectral whitening and 1-bit amplitude normalization, following the approach of

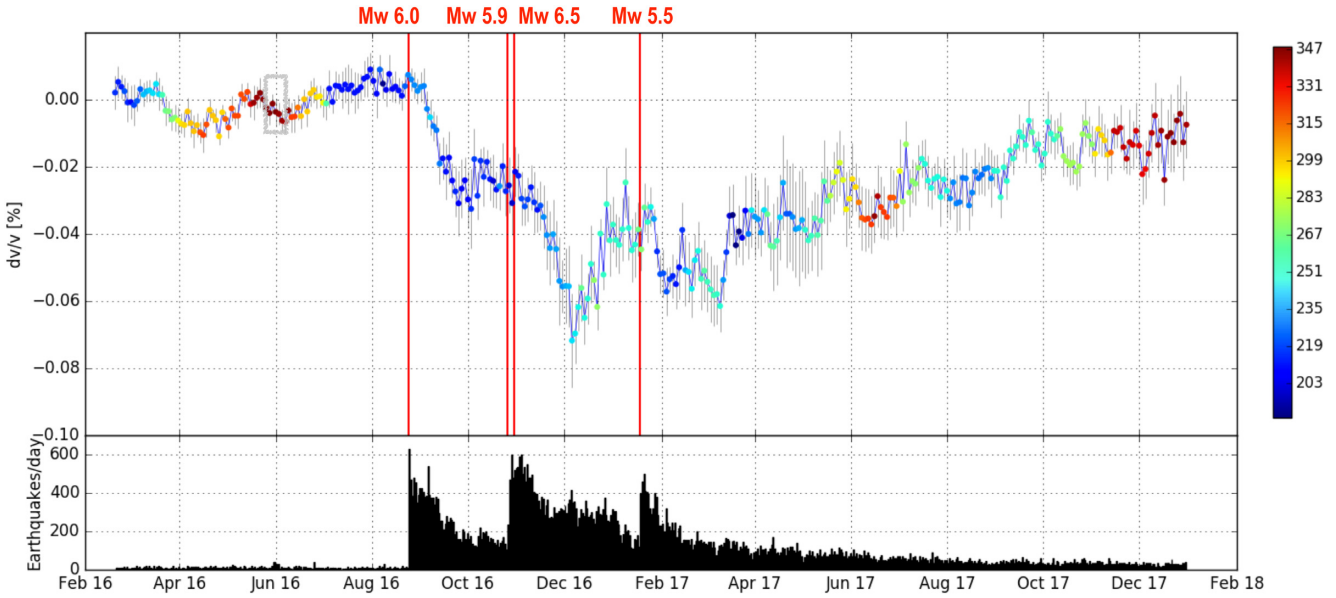

Figure 2. Top panel: relative velocity variations measured from CC of ambient noise recorded by the 28 stations shown in map, assuming as a reference the CC relative to the time interval 1 January−23 August 2016 (preceding the beginning of the central Italy sequence). Colours represent the number of station pairs considered in the computation, vertical bars indicate the uncertainties of the measurements. The vertical red lines highlight the time of occurrence of the four $M_w \geq 5.5$ main shocks. The grey rectangle marks the values of the dv/v taken as a reference for the computation of the velocity drop shown in Fig. 4. Bottom panel: number of earthquakes/day occurred in the area under study (Fig. 1) between 2016 and 2017 (from the INGV database available online at http://terremoti.ingv.it).

Table 1. Values of the parameters describing the different curves used to fit the postseismic relative velocity curve of Fig. 3. The corresponding values of *AIC* are evaluated to select the best-fitting models.

Fit with periodicity of 12 months		
Intercept	$(-42 \pm 5) \times 10^{-5}$	AIC= −2480
Linear	$(6 \pm 3) \times 10^{-7}$	
Logarithm	$(2 \pm 2) \times 10^{-5}$	
Periodicity sine	$(-1 \pm 2) \times 10^{-5}$	
Periodicity cosine	$(-1 \pm 1) \times 10^{-5}$	
Fit with linear and logarithmic terms		
Intercept	$(-43 \pm 3) \times 10^{-5}$	AIC= −2480
Linear	$(8 \pm 1) \times 10^{-7}$	
Logarithm	$(1.4 \pm 1.0) \times 10^{-5}$	
Fit with linear term only		
Intercept	$(-389 \pm 7) \times 10^{-6}$	AIC= −2475
Linear	$(9.1 \pm 0.5) \times 10^{-7}$	
Fit with logarithmic term only		
Intercept	$(-62 \pm 2) \times 10^{-5}$	AIC= −2449
Logarithm	$(7.7 \pm 0.3) \times 10^{-5}$	

Zaccarelli *et al.* (2011). Spectral whitening in the band from 0.1 to 1.0 Hz is intended to reduce the effects of temporal changes in the microseismic sources (Shapiro *et al.* 2006), while 1-bit normalization (Shapiro & Campillo 2004) should help to remove irregular events like earthquakes and improve the temporal stability of the noise records before cross correlation.

We calculate the hourly cross-correlation functions using the vertical component of the station pairs and consider the coda of the CCs from the arrival of the direct waves (group velocities slower than 2.5 km s^{-1}) up to a length of 50 s and in the frequency band from 0.1 to 0.9 Hz. At these frequencies and lag times, the depth sensitivity of the seismic coda waves to velocity perturbations can be considered similar to the surface wave sensitivity (Obermann *et al.* 2013b, 2016). The depth sensitivity of the phase velocity of Rayleigh wave to a shear wave velocity perturbation (Froment *et al.* 2013) indicates that our measurements essentially characterize the first 8 km of the upper crust, even if they are mostly sensitive to the top few kilometres.

To measure the relative velocity changes (dv/v) of surface waves from time delays in different time windows, two techniques are mostly used: the stretching method, which operate in the time domain by determining the parameter that maximizes the correlation between the two waveforms, and the Moving Window Cross-Spectrum analysis, first applied to earthquake coda waves (Poupinet *et al.* 1984) and then to CC codas (Brenguier *et al.* 2008; Clarke *et al.* 2011; Zaccarelli *et al.* 2011), where the time delay is computed in the frequency domain using the cross spectrum of the windowed wave front segments. We adopt this latter approach, and compare for each station pair a single reference CC—obtained from stacking all available hourly CCs for this pair in the period preceding the seismic sequence onset—with many subsequent current functions—obtained from stacking 50 d of CC (representative of the state of the crust for a given short period of time), within a set of 2-d sliding time windows. In a first approximation (i.e. supposing a homogeneous perturbation), the measured delays are a linear function of time, with slope corresponding to the relative time perturbation, opposed in sign to the actual dv/v, which are then estimated via a linear regression of the delay times.

Finally, we merge the delays measured from all the station pairs by computing the median value, and through a linear regression we obtain an estimate of dv/v representative of the entire crustal volume encircled by the seismic network.

3 TEMPORAL EVOLUTION OF RELATIVE SEISMIC VELOCITY

In Fig. 2(top) we show the relative velocity changes obtained from the analysis of the ambient noise CC between all combination of

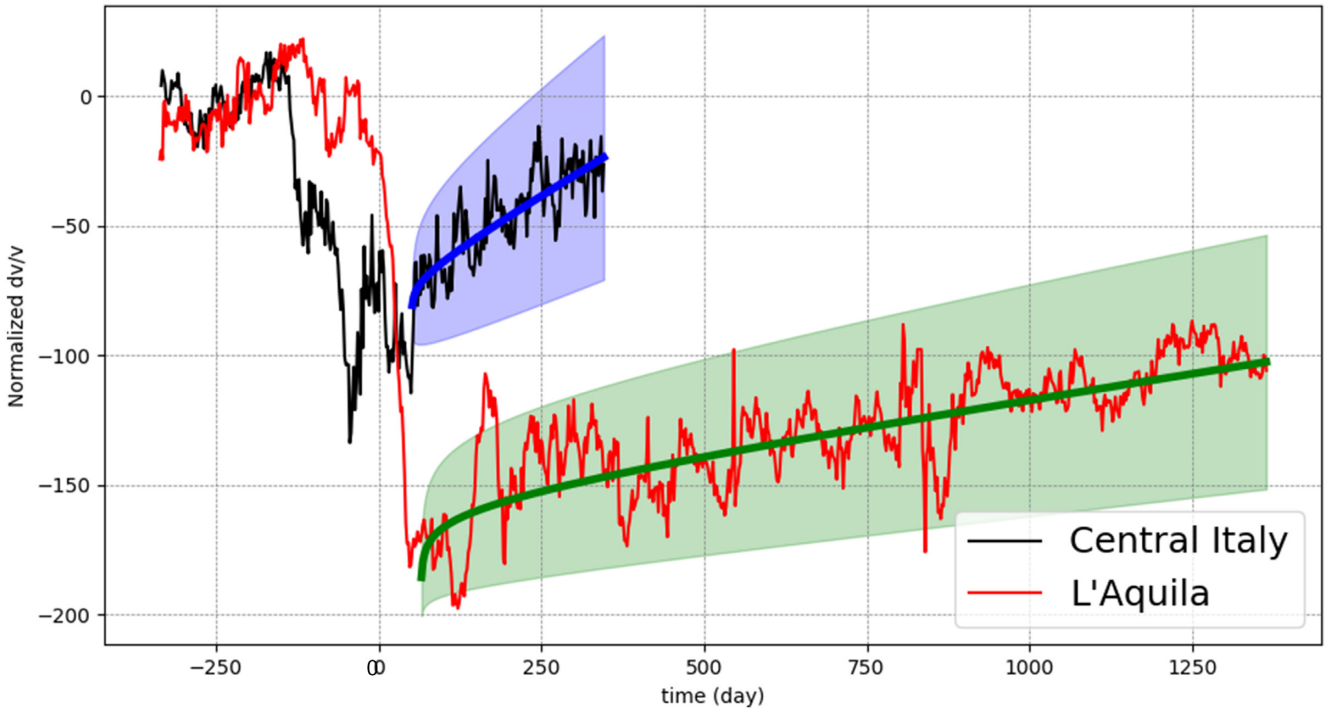

Figure 3. Crustal velocity variations relative to the 2016–2017 Central Italy earthquakes (black line), as in previous figure, and computed by Soldati *et al.* (2015) for the L'Aquila seismic sequence of 2009 (red). The dv/v values are normalized to the maximum amplitude of the time-series, shifted in time in order to syncronize the occurrence of the two main shocks of 6 April 2009 and 18 January 2017 (the latest of the central Italy sequence) at $t = 0$, and shifted vertically so that the average pre-seismic level of the two curves may overlap. The post-seismic relative velocity curves were fitted to differently parametrized functions, and the best-fitting models plotted in blue and green for the Central Italy and L'Aquila sequence, respectively (along with their associated errors in light blue/light green).

stations pairs. At each value of relative velocity change (plotted at the end of the 50-d interval with its associated errorbar), and a colour which corresponds to the number of station pairs involved in the estimate of dv/v, with a minimum of three pairs) to get an estimate. The vertical red lines highlight the time of occurrence of the four $M_w \geq 5.5$ main shocks, while the daily number of ($M_L \geq 1$) earthquakes belonging to the 2016–2017 central Italy sequence are plotted in Fig. 2(bottom). Seismic data are taken from the INGV database (available online at http://terremoti.ingv.it).

As reported in many previous studies of coseismic velocity variations (Wegler & Sens-Schönfelder 2007; Brenguier *et al.* 2008; Chen *et al.* 2010; Wang *et al.* 2017) we observe an abrupt decrease of relative seismic velocities as a result of the first earthquake's main shock (M_w 6.0 of 24 August 2016), with drop in velocity of the order of 0.04 per cent. The coseismic effect of the October 26 and October 30 events is again a sudden velocity drop of about 0.05 per cent, which rapidly recovered almost entirely before the main shock of 18 January 2017. This latter event was followed by a less pronounced (0.025 per cent) velocity reduction, which appears to quickly increase towards pre-earthquake conditions according to an apparently linear trend.

3.1 Post-seismic trend of relative seismic velocity

We focus here on the postseismic phase, with the aim of understanding what process drove the recovery of the coseismic velocity variations. The observed linear drift of the dv/v is indeed difficult to interpret because its temporal evolution is not consistent with the common mechanisms invoked to explain post-seismic deformation (viscoelastic rebound, frictional afterslip, fluids diffusion). In addition, this is motivated by a comparison with the analyses of the 2009 L'Aquila earthquake sequence conducted by Soldati *et al.* (2015) using the same ambient-noise-based approach.

We fit the velocity variation curve of Fig. 2 by a function consisting of a constant offset, a linear term, a logarithmic term and a seasonal variation (with period of 1 yr) or a combination of them (neglecting periodicity, linearity or the logarithmic trend).

The best-fitting model is selected using both Akaike's Information Criterion [*AIC*, Akaike (1974)], which determines the simplest model that explains the data best with as few parameters as possible, and the level of significance of the parameters. The parameters of the different fitting curves are given in Table 1, which shows that two models achieve the best fit (the lowest value of *AIC*): the one describing the dv/v as a combination of all the terms and the one where periodicity is not taken into account.

Noise-based crustal seismic velocity changes are indeed affected by external perturbations, such as rainfall, atmospheric pressure loading, and temperature changes that may mask the effects of tectonic processes, but their characteristic 1-yr periodicity is not detectable from the analysis of our 9-month long time-series, since it can only reveal periodicity on smaller length scale. It seems in fact that a-few-month periodicity is affecting our time-series, but repeating our computations of the delay times from a current CC obtained by stacking a smaller number of days (20 instead of 50) of CCs, we get a curve with similar trend to the one of Fig. 2, but with no apparent periodicity. We show it in Fig. S3. We therefore choose as the best model the one which does not include in the fitting function the periodic term (also because of the less parameters involved), and show it in Fig. 3 (blue) with its associated error (light

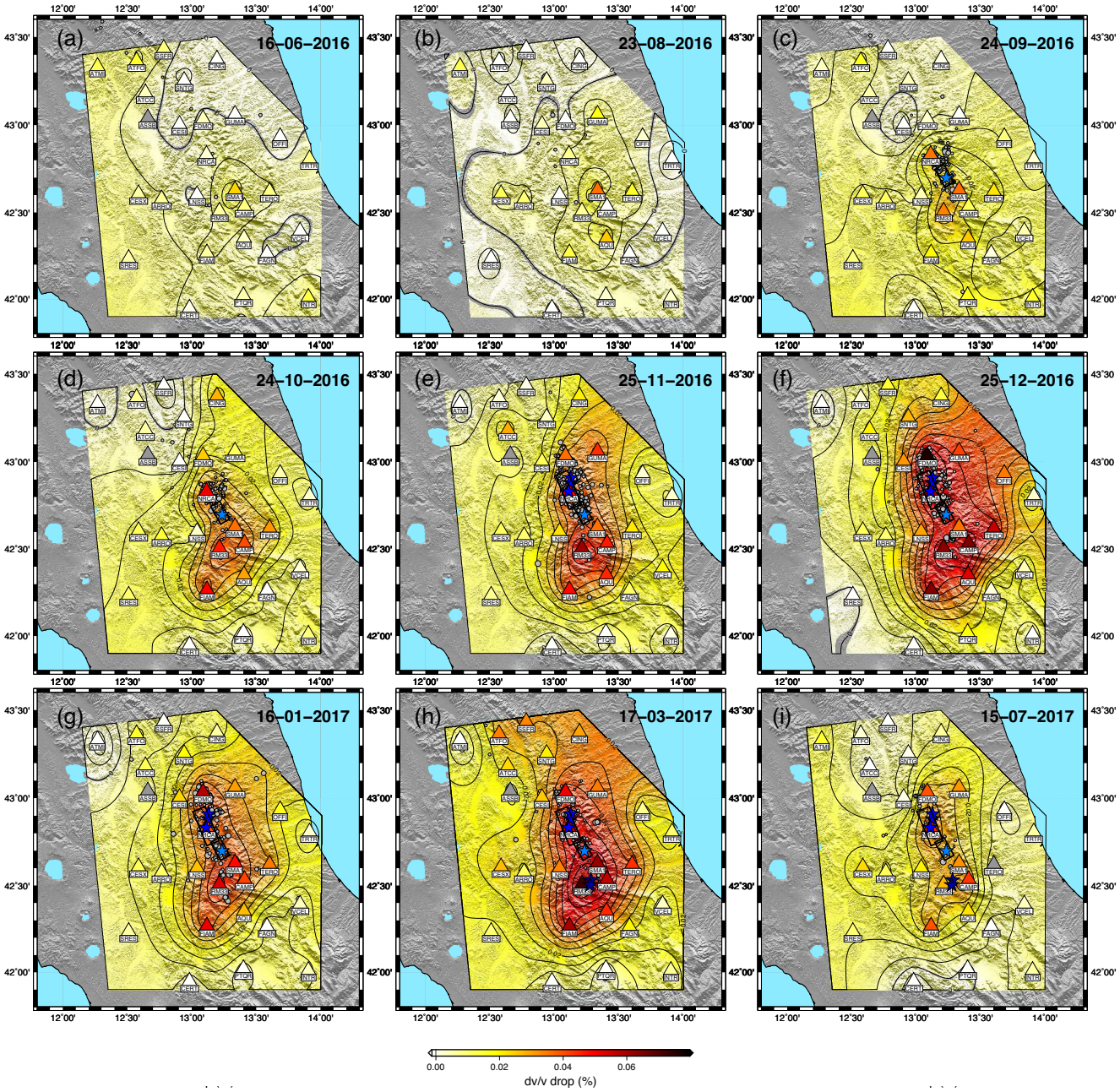

Figure 4. Map of the relative drop in velocity variations (per cent) obtained as average over 10 d (the day in the title denotes the last of the 10 d considered) with respect to the reference period of 26 May–4 June 2016 (where velocity variations are particularly well constrained). The blue stars represent the epicentres of the earthquakes with $M_w \geq 5.5$ and the black rectangles the fault planes projection. Each triangle denotes a station, with colour representing the value of the velocity drop computed as an average on all the baselines connecting that station with all the other ones. Grey triangles refer to stations where the velocity change cannot be computed due to gaps in the records. The colour map results from a Gaussian interpolation of the values of velocity change computed at the single stations.

blue) along with the postseismic relative velocity measurements (black). It appears to be dominated by a linear trend, as confirmed by the results of the regression test (Table 1): including in the fitting function a single component at a time, the linear component of the fitting function gets a fit only slightly worse than that obtained by the two best-fitting models.

The description of the post-seismic trend of velocity variations via a combination of linear and logarithmic functions is in agreement with what was obtained by Soldati *et al.* (2015) in their paper on L'Aquila 2009 earthquake, and suggests the idea that both afterslip and viscoelastic relaxation may be responsible of the velocity recovery. The difference with the L'Aquila case is that the post-earthquake healing rate is now much faster. This is evident from the visual comparison of the post-seismic trend of the dv/v of these two cases (Fig. 3), where red and black lines refer to the 2009 L'Aquila earthquake sequence and to the 2016–2017 central Italy sequence, respectively. The values of the relative velocity variations are normalized to the maximum amplitude of the time-series, and

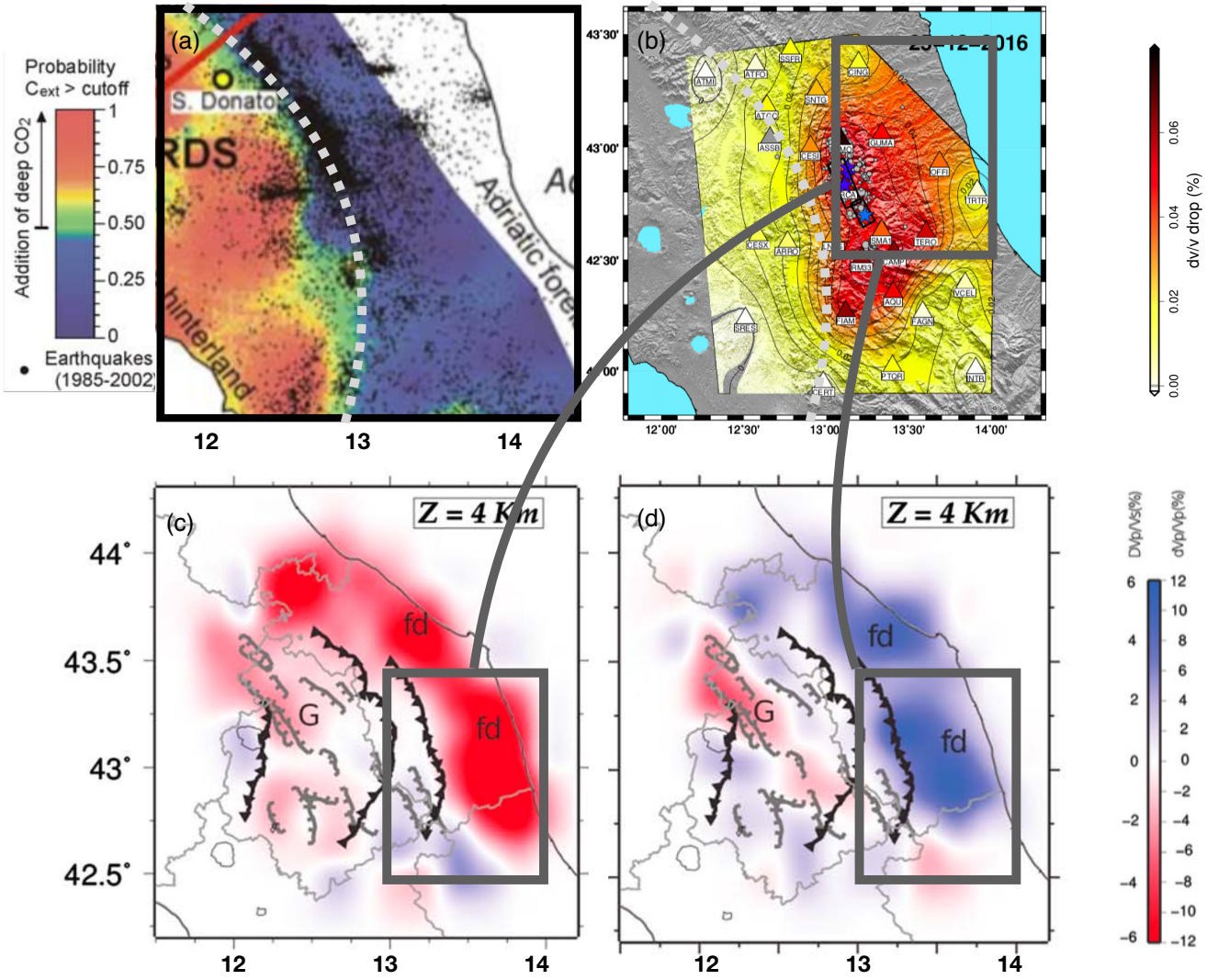

Figure 5. (a) Map of the CO_2-degassing area adapted from Chiodini *et al.* (2004) and (b) of the maximum extension of the relative drop in velocity variations from Fig. 4(f). The light grey dotted line indicates the eastern boundary of the CO_2-degassing area (left-hand panel) and the western limit of the region with high velocity drop (right-hand panel). Tomographic maps of v_P velocity (c) and v_P/v_S ratio (d) derived by Carannante *et al.* (2013) for a crustal depth of 4 km (adapted from their referred paper). Grey rectangles represent the same area on the maps (b)–(d).

shifted in time in order to synchronize the time of occurrence of the main shocks (6 April 2009 and 18 January 2017) in the two cases. The rapid increase of relative velocity after the main shock of January 2017 is even more important compared to the one following L'Aquila earthquake, if we consider that in this latter case the dv/v time-series is still far from the pre-earthquake level: Fig. 3 shows in fact that only about 30 per cent of the velocity perturbation is recovered after 4 yr from the L'Aquila main shock, versus a 75 per cent recovery after 1 yr from the latest main shock of the central Italy sequence. The best-fitting functions obtained in the two cases (green and blue lines) and their associated errors (light green/light blue) are shown in order to highlight the difference in the dv/v slope. It is important to notice that comparing time-series with different lengths may introduce a bias: computing the slope of the linear regression over just 300 d from the main shocks of the two sequences, we find in fact similar values. To draw robust conclusions about this comparison it will be thus necessary to repeat this test with a longer time-series of the dv/v associated to the central Italy earthquakes.

The mechanism by which seismic velocities decrease in response to stress perturbations is commonly described as related to the opening of cracks (Adams & Williamson 1923; Lockner 1977) which might possibly induce an increase in permeability and a transfer of fluids at depth. It has been shown (Miller *et al.* 2004; Lucente *et al.* 2010; Chiarabba *et al.* 2015) that fluids played a key role in the genesis and evolution of the seismic sequences of the Apennines (e.g. Colfiorito 1997; L'Aquila 2009), where the occurrence of multiple main shocks sequences is favoured by overpressurized fluids within the carbonate rocks (Di Luccio *et al.* 2010; Malagnini *et al.* 2012).

We think that whether the difference in the post-seismic trend we retrieve after series of earthquakes occurring in two different portions of the Apenninic belt may reflect a difference in the amount of fluids and/or in their ease of transfer. The major structural difference between the regions affected by the seismic sequences of L'Aquila 2009 and Amatrice-Visso-Norcia 2016–2017 is that the first one is on a carbonate platform (Parotto *et al.* 2004), characterized by large quantities of fluids, while the other lays on a sedimentary basin, including hybrid zones less rich in fluids. This has an effect

on the cracks generated by the faults rupture: they may open and close rapidly because the fluids-pore pressure does not contribute to the rate of fracturation. Indications about the fluids content are also given by Chiarabba *et al.* (2018), who observed high v_P/v_S within the upper portion of the 2016–2017 fault system, confined by the Sibillini thrust, indicating high pore pressure potentially responsible for triggering of aftershocks; and low v_P/v_S anomalies in the southern edge of the activated system, suggesting a limited fluid pressurization in this region. Finally, Tung & Masterlak (2018) showed, through a modelling of the Coulomb Failure Function (e.g. Harris & Simpson 1992; Reasenberg & Simpson 1992; King *et al.* 1994) and poroelasticity, that the M_w 5.9 Visso earthquake of 30 October 2016 has been triggered by the M_w 6.0 Amatrice event of 24 August 2016, and that this triggering can be modelled assuming high permeability, typical of very fractured rocks, and fast-traveling fluids.

The combined effect of a lower fluid content (with respect to the area surrounding L'Aquila main shock of 2009) and high rocks permeability, allowing quick circulation, may favour a fast recovery of the damaged crust in the region interested by the 2016–2017 seismic sequence. Moreover, while during the seismic sequence of 2009 most of the earthquakes affected a restricted region around the town of L'Aquila, preventing it from a quick recovery after the first main shock, the 2016–2017 sequence has been characterized by multiple major earthquakes which shifted the focus of the seismicity from Amatrice (after 2 months) towards the north direction and then (in January 2017) to the south, allowing a more rapid process of crack closure, stress relaxation and transfer of fluids, as confirmed by the results of Tung & Masterlak (2018) mentioned above.

4 MAPS OF RELATIVE SEISMIC VELOCITY DROP

To estimate the extent of the area affected by the crustal damage, and to visualize how it evolved over time as a consequence of subsequent main shocks, we map in Fig. 4, the spatial distribution of the drop in relative velocity variations computed on different dates preceding and following the occurrence of the 4 largest main shocks within the sequence.

The drop in velocity is computed as the difference between the average velocity change over 10 d (the day in the title of each panel denotes the last of the 10 d considered) and the value achieved by averaging the velocity variations throughout the period from 26 May to 4 June 2016, when the retrieved velocity variation estimates are almost constant to pre-sequence values, and particularly robust due to the high number of station pairs available. Coloured triangles represent the velocity drop at each station, computed by averaging the values corresponding to all the station pairs that include that particular station. Grey denotes stations not included in the computations due to technical reasons, for example gaps in the recordings. The map is obtained by interpolation of the single-station values with the aid of a Gaussian filter (Bracewell 1965).

We observe (Figs 4a and b) almost stationary conditions for drop values during the months preceding the M_w 6.0 main shock of 24 August 2016. After this event, the velocity drop begins to increase in a small region in proximity of the activated fault and south of it (Fig. 4c). A further increase of drop values appears before the occurrence of the M_w 5.9 and M_w 6.5 earthquakes of October 2016 (Fig. 4d). Following these two major events, the velocity drop area gradually broadens in the N–NE direction up to 50–60 km from Amatrice (Fig. 4e), until reaching its maximum values and extension at the end of December 2016 (Fig. 4f). After that, we find a partial recovery of the seismic velocity drop until mid-January 2017 (Fig. 4g), before the reactivation of the seismic sequence in the region around Campotosto town. A further intensification and widening of the velocity drop zone is observed in mid-March (Fig. 4h) as a consequence of the effect of the January events; then a non-negligible relative velocity decrease persists until at least mid-July, when it starts to fade out (Fig. 4i).

Given the relative sparsity of the stations' network, and the difficulty in merging together in a consistent way velocity measurements referring to stations with very different distance from each other and from the epicentral region, we regard this maps as a general indication on the spatial distribution of the velocity drop rather than a precise definition of the damaged area borders. With this in mind, our findings can be summarized into two main points. The first is that the spatial distribution of velocity drop has a well defined asymmetric pattern, covering the area surrounding the activated fault system and elongating towards the N–NE direction from it, and observable from November 2016 until June 2017. The second is the observation that the main shocks of 26 and 30 October 2016 and 18 January 2017 (and partially the one of August 24, even if in this case the result is not robust enough) occurred on areas previously affected by strong velocity reduction. This provides an indication that regions of the crust possibly damaged by previous earthquakes become so sensitive to stress variations to show clear changes in relative velocity even prior to the occurrence of subsequent seismic events.

The asymmetry of the maps in Fig. 4 can be the result of either a pre-existing heterogeneous tectonic and/or geologic setting or the effect of transient processes induced by the sequence of earthquakes, like fluids migration, pore pressure changes and crust fracturation. We thus investigate their potential correlation with maps describing lithology/geology, seismic tomography and the abundance/scarsity of fluids in the rocks.

Chiodini *et al.* (2004) observed an anomalous flux of CO_2 along the Tyrrenic hinterland which suddenly disappears in the Apenninic belt, where the gas accumulates in deep crustal traps generating overpressurized reservoirs. Their map of Fig. 5(a) highlights an intriguing coincidence among the zone where the seismicity of Apennines is concentrated and the eastern boundary of the CO_2 degassing areas, which in turn correlates well with the western boundary of the maximum extension of the relative velocity drop (Figs 4f or 5b). The supposed abundance of CO_2-rich fluids in a region of strong velocity drop would be in agreement with the high susceptibility to stress variations of the fluid rich zones observed by Brenguier *et al.* (2014) after the 2011 M_w 9.0 Tohoku-Oki earthquake. Unfortunately, since the ascent of deep fluids is only observed in the axial and internal chain zones, while it is absent in the Adriatic foreland, it cannot explain the asymmetric distribution along the NE direction of the dv/v drop.

The tomographic maps of v_P velocity and v_P/v_S derived by Carannante *et al.* (2013) for a crustal depth of 4 km (Figs 5c and d, adapted from their referred paper) show a low-velocity structure elongated for about 130 km in the NE–SW direction, corresponding to a high v_P/v_S anomaly with the same shape, that partially overlaps with the maximum extent area of the seismic velocity drop we retrieved (Fig. 5a). Given that overpressurized fluids are usually defined by high v_P/v_S anomalies in the upper crust (Dvorkin *et al.* 1999; Chiarabba *et al.* 2009), the slow velocity and high v_P/v_S body seen by tomography may be interpreted as a region of hydrated sediments. This is consistent with an explanation of the velocity reduction in terms of the dynamic effect of the major earthquakes

of the sequence on these highly porous sandstones: the passage of surface wave trains increases the pore pressure, triggering a pore opening effect; as a result, both v_P and v_S decrease, with $dv_S > dv_P$. The mechanism is the same responsible for the dynamic triggering of seismicity (Gomberg & Johnson 2005) and for the post-seismic hydrological variations in the carbonate aquifers (see Esposito *et al.* 2001) for the effect of the 1980 Irpinia earthquake).

5 SUMMARY

We applied noise-based techniques to monitor the temporal and spatial variation of crustal seismic velocities in central Italy in response to the earthquake sequence of 2016–2017. The analysis is conducted by cross-correlating continuous recordings of 2 yr of ambient noise from 28 stations located within 90 km of Amatrice, and by computing the CC functions between stations.

Seismic velocity perturbations show offsets corresponding to the occurrence of the major earthquakes of the sequence, after which they start to recover towards pre-earthquake conditions following an almost linear trend.

A test of the best-fitting function (in terms of *AIC*) of the post-seismic velocity variation curve results in a model consisting of a sum of a linear and a logarithmic term, with the first one neatly predominant, being capable of explaining most of the fit. This linear trend has been reported also in the case of the seismic sequence of L'Aquila 2009. However, contrary to the L'Aquila event, we here observe a very rapid post-earthquake fault-healing process, with at a recovery of about 75 per cent of the total seismic velocity drop within 1 yr from the latest main shock of 18 January 2017. We interpret this result as the effect of the faster circulation of the underground fluids, which are less abundant in the region affected by the 2016–2017 earthquake sequence with respect to the southern portion of the Apennines where L'Aquila is located, mainly consisting of a carbonate platform. In fact, assuming that the reduction in seismic velocities in response to an earthquake is caused by the opening of cracks, the induced crustal damage will last longer if these cracks remain open because internally pressurized by the fluids flux.

Fluids play a role also in the explanation of the retrieved asymmetry in the spatial maps of the relative velocity drop: the stronger velocity decrease in the region N–NE of the ruptured faults may indeed be correlated to the presence of highly porous and hydrated sediments in the foredeep basin, which respond dynamically to the passage of seismic waves by increasing the pore pressure, with consequent decreasing of seismic velocity.

ACKNOWLEDGEMENTS

GMT software (Wessel & Smith 1998) and Matplotlib software (Hunter 2007) were used to draw the figures. We are very grateful to D. Melini, for maintaining the high-performance computing centre of INGV (Rome), on which all computations were performed, and to P. Danecek, for his assistance in technical problems. We thank A. Michelini, A. Obermann and two anonymous reviewers for their helpful and constructive comments that greatly contributed to improve this paper.

REFERENCES

Adams, L.H. & Williamson, E.D., 1923. The compressibility of minerals and rocks at high pressures, *J. Franklin Inst.,* **195,** 475–529.

Akaike, H., 1974. A new look at the statistical model identification, *IEEE Trans. Autom. Control,* **19,** 716–723.

Bracewell, R., 1965. *The Fourier Transform and its Applications,* McGraw-Hill.

Brenguier, F., Campillo, M., Hadziioannou, C., Shapiro, N.M., Nadeau, R.M. & Larose, E., 2008. Postseismic relaxation along the San Andreas fault at Parkfield from continuous seismological observations, *Science,* **321,** 1478–1481.

Brenguier, F., Clarke, D., Aoki, Y., Shapiro, N.M., Campillo, M. & Ferrazzini, V., 2011. Monitoring volcanoes using seismic noise correlations, *C. R. Geosci.,* **343**(8-9), 633–638.

Brenguier, F., Campillo, M., Takeda, T., Aoki, Y., Shapiro, N.M. & Briand, X., 2014. Mapping pressurized volcanic fluids from induced crustal seismic velocity drops, *Science,* **345,** 80–82.

Carannante, S., Monachesi, G., Cattaneo, M., Amato, A. & Chiarabba, C., 2013. Deep structure and tectonics of the northern-central Apennines as seen by regional-scale tomography and 3-D located earthquakes, *J. geophys. Res.,* **118,** 5391–5403.

Chen, J.H., Froment, B., Liu, Q.Y. & Campillo, M., 2010. Distribution of seismic wave speed changes associated with the 12 May 2008 Mw 7.9 Wenchuan earthquake, *Geophys. Res. Lett.,* **37,** L18302.

Chiarabba, C. *et al.*, 2009. The 2009 L'Aquila (central Italy) MW 6.3 earthquake: main shock and aftershocks, *Geophys. Res. Lett.,* **36,** L18308.

Chiarabba, C., De Gori, P. & Mele, F.M., 2015. Recent seismicity of Italy: active tectonics of the central Mediterranean region and seismicity rate changes after the Mw 6.3 L'Aquila earthquake, *Tectonophysics,* **638,** 82–93.

Chiarabba, C., De Gori, P., Cattaneo, M., Spallarossa, D. & Segou, M., 2018. Faults geometry and the role of fluids in the 2016-2017 Central Italy seismic sequence, *Geophys. Res. Lett.,* **45**(14), 6963–6971.

Chiaraluce, L. *et al.*, 2017. The 2016 Central Italy seismic sequence: a first look at the mainshocks, aftershocks, and source models, *Seismol. Res. Lett.,* **88**(3), 757–771.

Chiodini, G., Cardellini, C., Amato, A., Boschi, E., Caliro, S., Frondini, F. & Ventura, G., 2004. Carbon dioxide Earth degassing and seismogenesis in central and southern Italy, *Geophys. Res. Lett.,* **31**(7), L07615, doi:10.1029/2004GL019480.

Clarke, D., Zaccarelli, L., Shapiro, N. & Brenguier, F., 2011. Assessment of resolution and accuracy of the moving window cross spectral technique for monitoring crustal temporal variations using ambient seismic noise, *Geophys. J. Int.,* 1–16, doi:10.1111/j.1365–246X.2011.05074.x.

Devoti, R. *et al.*, 2017. A combined velocity field of the Mediterranean region, *Ann. Geophys.,* **60**(2), doi:10.4401/ag-7059.

Di Luccio, F., Ventura, G., Giovambattista, R.D., Piscini, A. & Cinti, F.R., 2010. Normal faults and thrusts reactivated by deep fluids: the 6 April 2009 Mw 6.3 L' Aquila earthquake, central Italy, *J. geophys. Res.,* **115,** B06315.

Dvorkin, J., Mavko, G. & Nur, A., 1999. Overpressure detection from compressional- and shearwave data, *Geophys. Res. Lett.,* **26**(22), 3417–3420.

Esposito, E., Pece, R., Porfido, S. & Tranfaglia, G., 2001. Hydrological anomalies connected to earthquakes in southern Apennines (Italy), *Nat. Hazards Earth Syst. Sci.,* **1,** 137–144.

Froment, B., Campillo, M., Chen, J.H. & Liu, Q.Y., 2013. Wenchuan earthquake from seismic ambient noise monitoring, *Geophys. Res. Lett.,* **40,** 78–82.

Gomberg, J. & Johnson, P., 2005. Dynamic triggering of earthquakes, *Nature,* **437,** 830, doi:10.1038/437830a.

Harris, R.A. & Simpson, R.W., 1992. Changes in static stress on southern California faults after the 1992 Landers earthquake, *Nature,* **360**(6401), 251–254.

Hobiger, M., Wegler, U., Shiomi, K. & Nakahara, H., 2012. Coseismic and postseismic elastic wave velocity variations caused by the 2008 Iwate-Miyagi Nairiku earthquake, Japan, *J. geophys. Res.,* **117,** B09313.

Hunter, J.D., 2007. Matplotlib: a 2D graphics environment, *Comput. Sci. Eng.,* **9**(3), 90–95.

King, G.C., Stein, R.S. & Lin, J., 1994. Static stress changes and the triggering of earthquakes, *Bull. seism. Soc. Am.,* **84**(3), 935–953.

Lockner, D.A., Walsh, J.B. & Byerlee, J.D., 1977. Changes in seismic velocity and attenuation during deformation of granite, *J. geophys. Res.,* **82,** 5374–5378.

Lucente, F., Gori, P.D., Margheriti, L., Piccinini, D., Bona, M.D., Chiarabba, C. & Agostinetti, N.P., 2010. Temporal variation of seismic velocity and anisotropy before the 2009 Mw 6.3 L'Aquila earthquake, Italy, *Geology,* **38**(n.11), 1015–1018.

Malagnini, L., Lucente, F.P., De Gori, P., Akinci, A. & Munafo, I., 2012. Control of pore fluid pressure diffusion on fault failure mode: insights from the 2009 L'Aquila seismic sequence, *J. geophys. Res.,* **117,** B5.

Marchetti, A. *et al.*, 2016. The Italian Seismic Bulletin: strategies, revised pickings and locations of the central Italy seismic sequence, *Ann. Geophys.,* **59,** doi:10.4401/ag-7169.

Marzorati, S., Cattaneo, M., Frapiccini, M., Monachesi, G. & Ladina, C., 2016. Recent seismicity before the 24 August 2016 Mw 6.0 central Italy earthquake as recorded by the ReSIICO seismic network, *Ann. Geophys.,* **59,** doi:10.4401/ag-7191.

Michele, M. *et al.*, 2016. The Amatrice 2016 seismic sequence: a preliminary look at the mainshock and aftershocks distribution, *Ann. Geophys.,* **59,** doi:10.4401/ag-7227.

Miller, S.A., Collettini, C., Chiaraluce, L., Cocco, M., Barchi, M. & Kaus, B.J.P., 2014. Aftershocks driven by a high-pressure CO_2 source at depth, *Nature,* **427,** 724–727.

Obermann, A., Planes, T., Larose, E. & Campillo, M., 2013. Imaging pre and co eruptive structural and mechanical changes of a volcano with ambient noise, *J. geophys. Res.,* **118,** 1–10.

Obermann, A., Planes, T. & Larose, E., 2013. Depth sensitivity of seismic coda waves to velocity perturbations in an elastic heterogeneous medium, *Geophys. J. Int.,* **37,** L18302.

Obermann, A., Planes, T., Hadziioannou, C. & Campillo, M., 2016. Lapse-time-dependent coda-wave depth sensitivity to local velocity perturbations in 3-D heterogeneous elastic media, *Geophys. J. Int.,* **207**(1), 59–66.

Parotto, M., Cavinato, G.P., Miccadei, E. & Tozzi, M., 2004. Line CROP 11: Central Apennines, *Mem. Descr. Carta Geol. It.,* **62,** 145–153.

Poupinet, G., Ellsworth, W.L. & Frechet, J., 1984. Monitoring velocity variations in the crust using earthquake doublets: an application to the Calaveras fault, California, *J. geophys. Res.,* **89,** 5719–5731.

Reasenberg, P.A. & Simpson, R.W., 1992. Response of regional seismicity to the static stress change produced by the Loma Prieta earthquake, *Science,* **255**(5052), 1687–1690.

Sanchez-Pastor, P., Obermann, A. & Schimmel, M., 2018. Detecting and locating precursory signals during the 2011 El Hierro, Canary Island submarine eruption, GRL, *Geophys. Res. Lett.,* **45**(2), doi:10.1029/2018GL079550.

Serpelloni, E., Anzidei, M., Baldi, P., Casula, G. & Galvani, A., 2005. Crustal velocity and strain-rate fields in Italy and surrounding regions: new results from the analysis of permanent and nonpermanent GPS networks, *Geophys. J. Int.,* **161,** 861–880.

Shapiro, N.M. & Campillo, M., 2004. Emergence of broadband Rayleigh waves from correlations of the ambient seismic noise, *Geophys. Res. Lett.,* **31,** L07614.

Shapiro, N.M., Ritzwoller, M.H. & Bensen, G.D., 2016. Source location of the 26 sec microseism from cross-correlations of ambient seismic noise, *Geophys. Res. Lett.,* **33,** L18310, doi:10.1029/2006GL027010.

Soldati, G., Zaccarelli, L., Faenza, L. & Michelini, A., 2015. Monitoring of crustal seismic velocity variations in the L'Aquila fault zone inferred from noise cross-correlation, *Geophys. J. Int.,* **202,** 604–611.

Taira, T. & Brenguier, F., 2016. Response of hydrothermal system to stress transients at Lassen Volcanic Center, California, inferred from seismic interferometry with ambient noise, *Earth, Planets Space,* **68,** 162.

Tung, S. & Masterlark, T., 2018. Delayed poroelastic triggering of the 2016 October Visso earthquake by the August Amatrice earthquake, *Geophys. Res. Lett.,* **45,** doi:10.1002/2017GL076453.

Wang, Q.-Y., Brenguier, F., Campillo, M., Lecointre, A., Takeda, T. & Aoki, Y., 2017. Seasonal crustal seismic velocity changes throughout Japan, *J. geophys. Res.: Solid Earth,* **122,** 7987–8002.

Wegler, U. & Sens-Schönfelder, C., 2007. Fault zone monitoring with passive image interferometry, *Geophys. J. Int.,* **168,** 1029–1033.

Wessel, P. & Smith, W., 1998. New, improved version of the generic mapping tools released, *EOS, Trans. Am. Geophys. Un.,* **79,** 579–579.

Zaccarelli, L., Shapiro, N.M., Faenza, L., Soldati, G. & Michelini, A., 2011. Variations of crustal elastic properties during the 2009 L'Aquila earthquake inferred from cross correlations of ambient seismic noise, *Geophys. Res. Lett.,* **38**(L24304), doi:10.1029/2011GL049750.

SUPPORTING INFORMATION

Supplementary data are available at *GJI* online.

Figure S1. Map of the central Apennines showing all the seismic stations available (black) from the Italian National Seismic Network (INSN) and of the Mediterranean Very Broadband Seismographic Network (*MedNet*); the ones selected in this study are marked in red.

Figure S2. Data availability from January 2016 to April 2017 (blue dots) for all the stations of Fig. S1. Red asterisks mark the 28 stations selected for this analysis.

Figure S3. Relative velocity variations measured from 20-d stacking of hourly CC of ambient noise recorded by the 28 stations shown in red in Fig. S1. Colours represent the number of station pairs considered in the computation, vertical bars indicate the uncertainties of the measurements. The vertical red lines highlight the time of occurrence of the four $M_w \geq 5.5$ main shocks as in Fig. 2.

Please note: Oxford University Press is not responsible for the content or functionality of any supporting materials supplied by the authors. Any queries (other than missing material) should be directed to the corresponding author for the paper.